An experimental and simulation study of heteroaggregation in a binary mixture of alumina and silica colloids

Anne Aimable, A Delomenie, Manuella Cerbelaud, Arnaud Videcoq, T. Chartier, Florian Boutenel, Thierry Cutard, Gilles Dusserre

An experimental and simulation study of heteroaggregation in a binary mixture of alumina and silica colloids

A. Aimable*[1], A. Delomenie[1], M. Cerbelaud[1], A. Videcoq[1], T. Chartier[1], F. Boutenel[2], T. Cutard[2], G. Dusserre[2]

[1] Univ. Limoges, CNRS, IRCER, UMR 7315, F-87000 Limoges, France

[2] Institut Clément Ader, Université de Toulouse, CNRS, IMT Mines Albi, INSA, UPS, ISAE-SUPAERO, Campus Jarlard, 81013 Albi CT Cedex 09, France

* Corresponding author:
Anne Aimable
E-mail : anne.aimable@unilim.fr
Phone : +33 (0) 587 50 23 68
Fax : +33 (0) 587 50 23 04

Graphical abstract

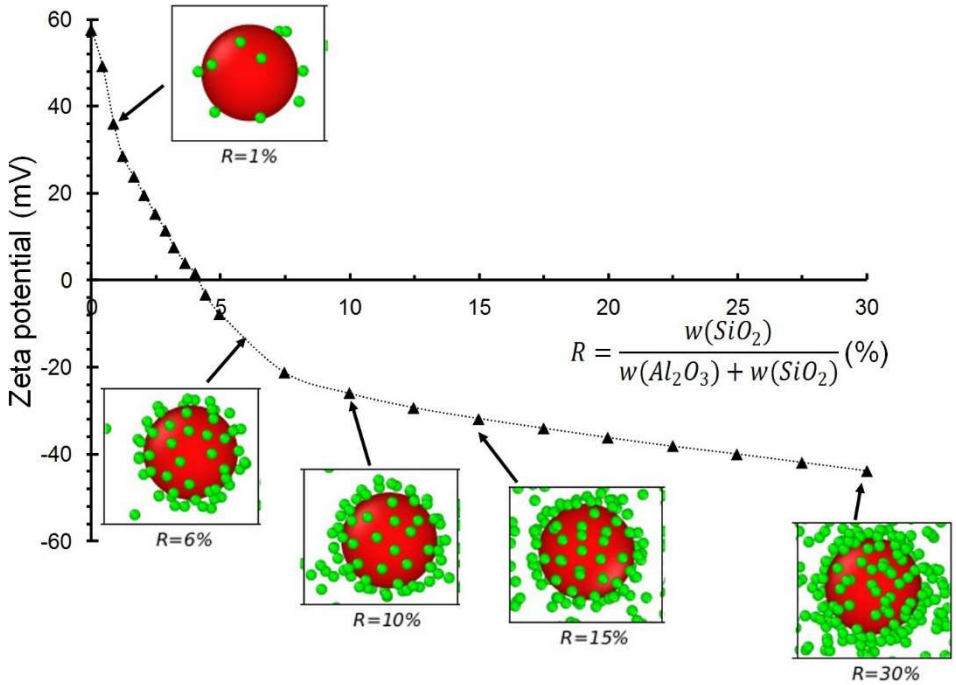

Abstract

Heteroaggregation corresponds to an attraction between two different types of particles. It can either lead to stable or instable systems, depending on the conditions. In this paper heteroaggregation in binary mixtures of alumina and silica colloids (size ratio = 8.5) is studied, by coupling an experimental approach and Brownian dynamics simulations. Two main objectives are targeted. The first one is to bridge the gap between coagulation and dispersion, by examining the effect of the relative concentrations of silica and alumina. The second one is to study the effect of the volume fraction of solid, which impacts strongly the aggregation mechanism.

The coagulation or the dispersion are evidenced by sedimentation tests, granulometry, and rheological measurements, supported by zeta potential measurements. Heteroaggregates could be observed by transmission electron microscopy. Brownian dynamics simulations give more insight into the very first moments of the process, to predict the adsorption kinetic and the heteroaggregates structure.

A very good agreement is obtained between experiments and simulations, which both show adsorption of silica leads to the bridging of alumina particles and thus coagulation at low concentration. This adsorption is rapidly limited by electrostatic interactions, then hindering alumina agglomeration by repulsive interactions. For the higher solid fractions, alumina aggregation is more likely, as two alumina particles can easier encounter before their surface is enough covered by the silica to avoid their aggregation.

Keywords

Heteroaggregation, Brownian dynamics simulation, Alumina, Silica, Colloidal suspension

1. Introduction

The stability of a colloidal suspension depends on the interactions that occur between the particles, and between the particles and the solvent. Colloids are subject to repulsive forces resulting from the interaction of electric double layers, and attractive van der Waals forces resulting from temporary dipoles. In addition, if the colloid size is small, the Brownian motion must be considered. D.L.V.O. theory (Derjaguin, Landau, Verwey, Overbeek) establishes the balance of the forces acting between the particles [1]. Stability is achieved when the repulsive forces are predominant, leading to a well-dispersed system, where the particles are individual

in suspension. On the contrary, an unstable suspension is observed when the attractive forces are predominant, leading to an agglomeration of the particles, and a rapid sedimentation.

When two types of particles are present in a suspension, several behaviors can be distinguished [2]:
- the absence of agglomeration, which corresponds to a co-dispersion of both types of particles, with repulsive forces predominant between all the particles,
- an homo-agglomeration between identical particles, the second remaining as a dispersed phase,
- the heteroaggregation, corresponding to an attraction between two different types of particles. The particles may differ from their composition, shape, size or surface charge. Heteroaggregation can either lead to a stable or instable system [3] [4].

Many different applications are based on a heteroaggregation process [5]. In water treatments, solid pollutants (plastics, metals) in the form of micro or nanoparticles are separated from the water by heteroaggregation [6] [7] [8]. Functionalized [9], raspberry or rough colloids [10], core-shell [11], or hybrid particles [12] [13], could be prepared by combining different types of colloids, to modify their surface chemistry or their shape. Their synthesis depends on a finely controlled heteroaggregation process. Their assembly give smart supraparticles [14] [15] [16], which may be of great interest for new materials such as metamaterials [17], colloidal crystals [18], or complex nanomachines [19]. Another field of application is the stabilization of emulsions by heteroaggregates [20] [21], which could replace efficiently the use of traditional organic surfactants, which are not healthy nor environmental-friendly. Finally the use of binary components mixtures and heteroaggregation was employed for advanced ceramics [22], to obtain a well-designed porosity for example [23] [24], or for biomimetic materials [25]. In parallel, some studies have proposed some kinetic models to describe and predict the coagulation process [26] [27] [28] [29].

The case of heteroaggregation of particles with a high size asymmetry has been particularly studied, as it allows the formation of very specific aggregate structures. Experimental parameters such as the size ratio, the relative concentration of the particles, the pH and the ionic strength, can strongly modify the final structure of the aggregates as well as the kinetic of aggregation [30]. Some phase diagram could be obtained with mixtures of polystyrene and silica suspensions, showing the transition from a stable fluid to an unstable gel behavior, with increasing nanoparticle concentration [31] [32]. A large amount of small particles can form a relatively dense layer at the surface of the large ones, and stabilize the suspension. On the contrary, when the small particles are not sufficient to obtain a coating of the large particles, they form bridges between them leading to coagulation, and the suspension is unstable.

Coupling experimental and simulation studies on bi-component system made of alumina and silica particles [33] [34] [35] contributed to the development of very performant models based on Brownian dynamics simulations [36] [37]. Most studies were conducted with a small ratio of silica colloids, leading to heterocoagulation. The influent parameters and the kinetic of the coagulation process were determined. A very innovative granulation method in dilute suspension was proposed as a direct application, leading to well-designed dense and porous ceramic millimetric beads [38] [39] [40] [41]. Another recent application was a biomimetic assembly silica-alumina nacre-like composite [25]. In the literature, the addition of inorganic colloidal sols was reported for the stabilization of ceramic slurries. Boehmite [42], colloidal silica [28] [43] [44], titania or zirconia [45], allow improving the stability of suspensions of alumina, silicon nitride or carbide, and reducing their viscosity. The interest of inorganic sols for ceramic dispersion is to substitute organic dispersants and thus limit possible problems during thermal treatments.

This paper presents a study of the heteroaggregation process by coupling experiments and Brownian dynamics simulations in binary mixtures of alumina and silica colloids. The coagulation or the dispersion are evidenced by sedimentation tests, granulometry, and rheological measurements, supported by zeta potential measurements. Heteroaggregates could be observed by transmission electron microscopy. The size asymmetry between alumina and silica is relatively high (size ratio = 8.5). Two main objectives are targeted. The first one is to bridge the gap between coagulation and dispersion, by examining systematically the effect of the relative concentrations of silica and alumina. The second one is to study the effect of the volume fraction of solid, which impacts strongly the aggregation mechanism. Brownian dynamics simulations give more insight into the very first moments of the heteroaggregation process, and predict with an extremely good accuracy the heteroaggregates structure obtained in these different conditions.

2. Experimental study

2.1. Materials

The alumina powder used in this study is the high-purity AKP50 from Sumitomo (Japan), which presents a specific surface area of 10.3 $m^2.g^{-1}$ (*supplier data*), and a homogeneous grain size distribution with a mean diameter equal to 206 ± 4 nm (Figure 1). The colloidal silica is a commercial suspension of Ludox AS40 (40 wt.% of SiO_2 in NH_4OH solution) from Grace Davison (USA). It is an opalescent white liquid. The particles are discrete uniform spheres of SiO_2, which have no internal surface area or detectable crystallinity. The specific surface area is 140 $m^2.g^{-1}$ (*supplier data*) with a mean particle size equal to 24 ± 2 nm (Figure 1). For the

preparation of the suspension, pH was adjusted by using HCl solution at a concentration 0.1M (Aldrich).

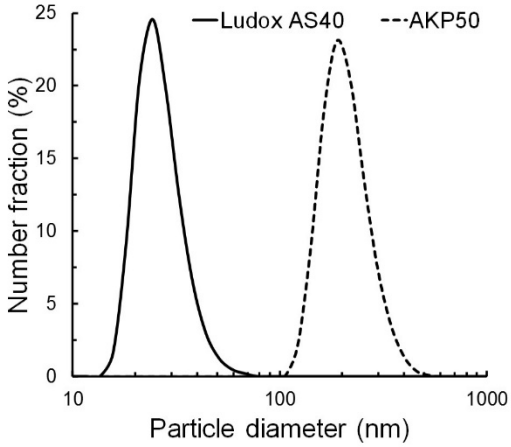

Figure 1: Particle size distribution of raw materials alumina AKP50, and silica Ludox AS40 (measurements done on 0.01wt.% suspensions, with Malvern Nanosizer ZS)

2.2. Experimental procedure

This study aims at investigating the conditions of heteroaggregation between colloidal silica and alumina, and better define the limits of coagulation and dispersion. Some mixtures of alumina and silica were prepared by varying the ratio R corresponding to the relative weight of silica compared to the total weight of solid in the suspension (in %), as defined in Equation 1.

$$R = \frac{w(SiO_2)}{w(Al_2O_3)+w(SiO_2)} * 100 \qquad \text{Equation 1}$$

The procedure for the preparation of the suspensions is presented in Figure 2.

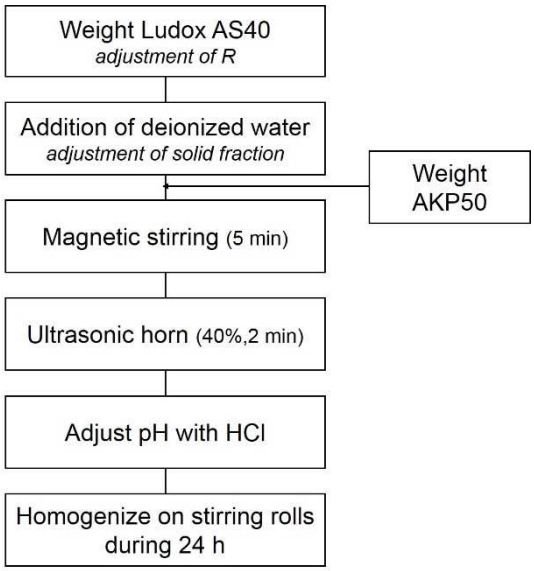

Figure 2: Procedure for the preparation of alumina/silica mixtures with various R

2.3. Characterization techniques

Zeta potential measurements were performed with an ESA analyser (AcoustoSizer II S flow through system, Colloidal Dynamics). The zeta potential was obtained from the ESA voltage data treated with the AcoustoSizer II operation software by using the O'Brien relationship. Zeta potential measurements were done on diluted alumina and silica suspensions, at 1.0 vol.%, in deionized water by varying pH with 1.0 mol/L HCl or NaOH addition with the automated AcoustoSizer II pH titration system. Zeta potential was also measured on a diluted alumina suspension (1.0 vol.%, pH preliminary set at 5.5) by addition of Ludox AS40 in order to vary the R ratio. In one case, Ludox AS40 was added at natural pH (9.2), and in another case the pH of the silica suspension was decreased at pH 7.5 by adding a small amount of HCl 0.1M, in order to limit the pH variation all over the titration.

Sedimentation experiments were performed, on a pure alumina suspension, and some mixtures of alumina and silica at different R ratios. The total solid fraction was 1.0 vol.%, and the pH of all the suspensions was set at 6.5. Immediately after preparation, the samples were allowed to settle in closed tubes for a total of 28 days. In such conditions, a clear supernatant was observed and the height of cake was measured accurately. The sediment height was reported as a percentage of the initial volume of suspension.

Laser diffraction analysis (Horiba LA-950) was used to determine the particle size distribution of suspensions of pure alumina and of mixtures of silica and alumina at different R ratios, and after 24 hours of preparation. The Mie method was applied using the refractive index of alumina

(n=1.77). The D_{v10}, D_{v50} and D_{v90} were extracted from the size distribution in order to compare the impact of R on the width of the distribution.

Rheological measurements were performed on the most stable suspensions using a stress-controlled rheometer ARG2 from TA Instruments (no sedimentation is allowed during such measurement). The measuring geometry consisted of a 20mm diameter upper plate and a Peltier lower plate. The gap was set to 1mm. Steady state flow measurements were performed. They consist of a series of creep experiments with varying shear rates, where the equilibrium shear stress is obtained when the curve reaches a linear regime. The following procedure of measurement was followed:

1. a pre-shear at shear rate of 10 s^{-1} during 30 s, and at 0.1 s^{-1} during 120 s,
2. a shear rate sweep from 0.01 s^{-1} to 200 s^{-1}

The morphology of the heteroaggregates was observed by Transmission Electron Microscopy (TEM, JEOL 2100F) after 24 hours of preparation.

2.4. Experimental results

Zeta potential measurements on diluted suspensions (1.0 vol.%) of alumina AKP50 and silica Ludox AS40 are reported in Figure 3. AKP 50 presents an isoelectric point (IEP) at 9.2. A high zeta potential absolute value above 30 mV is measured at acidic and neutral pH until the value 7.8, or at basic pH, above 10.8. A high absolute value of zeta potential corresponds to strong electrostatic forces between the particles in suspension, and thus to a good dispersion. Therefore, AKP50 should be preferentially dispersed in acidic conditions, and would present in such conditions a positive surface charge.

The IEP of Ludox AS40 is equal to 2.3. A high negative zeta potential is measured for pH values higher than 6.5, corresponding to the best conditions for silica dispersion.

Therefore, in a wide range of pH, silica and alumina present opposite surface charges. Heteroaggregation may occur from pH 2.3 to pH 9.2, with an optimum range corresponding to high zeta potentials of opposite sign, i.e. for pH comprised between 6 and 8.

In this study, mixtures of alumina and silica at different R ratios are prepared in that range of pH, and preferentially at a controlled pH of 6.5.

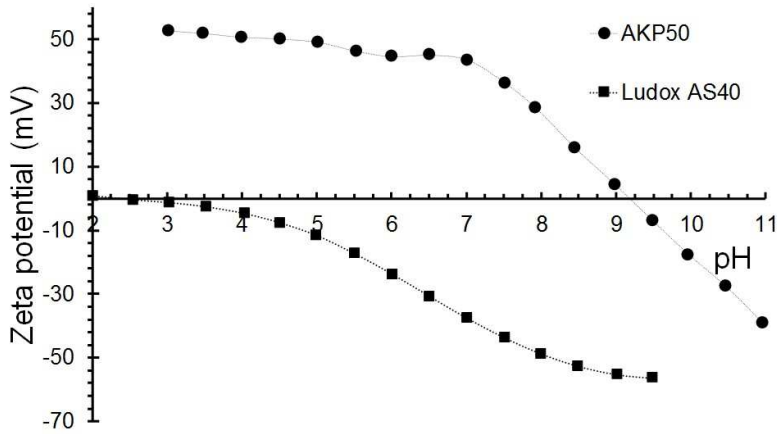

Figure 3: Evolution of the zeta potential as a function of the pH of alumina AKP50, and silica Ludox AS40 (1.0 vol.% in deionized water)

Zeta potential evolution of mixtures of alumina and silica was then measured as a function of R (Figure 4), in order to evaluate the influence of silica concentration. The pH of the alumina suspension was preliminary set to 5.5, corresponding to opposite charges between the two types of colloids, as explained previously. One measurement was done by adding Ludox AS40 at its natural pH (around 9.2) to the alumina suspension, and another one by adding Ludox AS40 at a pH preliminary set at 7.5. In both cases, zeta potential decreases when R increases. Silica particles, wearing negative surface charges, are attracted by the positive surface of alumina, leading to a decrease of the zeta potential. The addition of Ludox AS40 at natural pH 9.2 leads to a significant increase of the pH of the binary suspension, with a final pH value around 8.9 when R = 30%. At the same time, the zeta potential decreases strongly up to ζ = -30 mV for R=6%, changing sign at R = 2% (ζ = 0 mV). For R > 6%, zeta potential decreases more slowly to attain ζ = -52 mV for R = 30%. Addition of Ludox AS40 with an initial pH of 7.5 leads to a final pH of 7.5 for the binary suspension at R = 30%, and the pH variation is thus limited in a range where heteroaggregation is predominant. As in the previous case, a strong decrease of zeta potential is observed for the smallest values of R below 6% attaining ζ = -12 mV, with a sign reversal for R = 4%. A lower decrease is then observed for R > 6%, and a zeta potential of ζ = -44 mV is reached for R = 30%. The difference between the two curves is due to the lower surface charge of silica particles at a lower pH of 7.5. In both cases, a small addition of silica until R = 10% to an alumina suspension leads to a strong decrease of zeta potential, corresponding to an unstable and agglomerated system, whereas as soon as R is more than 10%, zeta potential is less than -30 mV, which is usually considered as a sufficient potential for a dispersed and stable system.

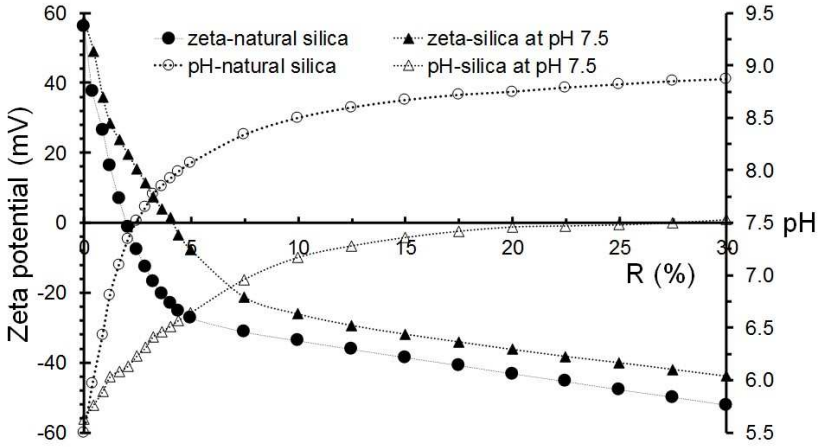

Figure 4: Evolution of the zeta potential and the pH of an alumina AKP50 suspension (initial pH = 5.5; 1.0 vol.%) as a function of R by adding Ludox AS40 at natural pH 9.2, and at a pH preliminary set at 7.5

Sedimentation was observed with suspension of alumina and silica for different R ratios, the pH value being set at 6.5 (Figure 5), after a time of 1 week, and 1 month. In these tests the solid fraction is low (1,0 vol%). A small deposit corresponds to well dispersed particles and a stable suspension, such as those observed for pure alumina at pH 6.5, and R = 12.5, 15, 20 and 30%. On the contrary, high deposits are formed rapidly for R = 1, 5, 7.5 and 10%, and their height decreases slightly between 1 week and 1 month, corresponding to a very small rearrangement of particles in the deposit. Therefore, for R ≤ 10%, silica acts as an agglomerating agent leading to an unstable suspension, whereas for R > 10%, a stable and non-agglomerated suspension is obtained.

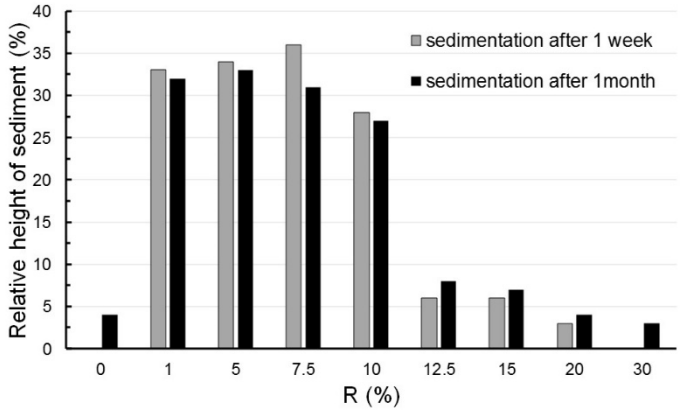

Figure 5: Relative height of the sediment measured in sedimentation tests for mixtures of alumina and silica (1.0 vol.%, pH = 6.5) with various R ratios, after 1 week and 1 month.

In order to characterize the presence and the size of these agglomerates, the particle size distribution of suspensions with different R is reported in Figure 6. High values for D_{50} and D_{90} are measured when R ≤ 10% (except for R = 0% - pure alumina), which corresponds to a strong agglomeration of the suspension. On the contrary, for R > 10%, D_{50} is around 0.2 µm, and D_{90} decreases gradually when R increases, showing a good dispersion of the elementary particles, with few agglomerates, their presence being eliminated when R > 25%. This result is in a very good correlation with the observations done through sedimentation tests.

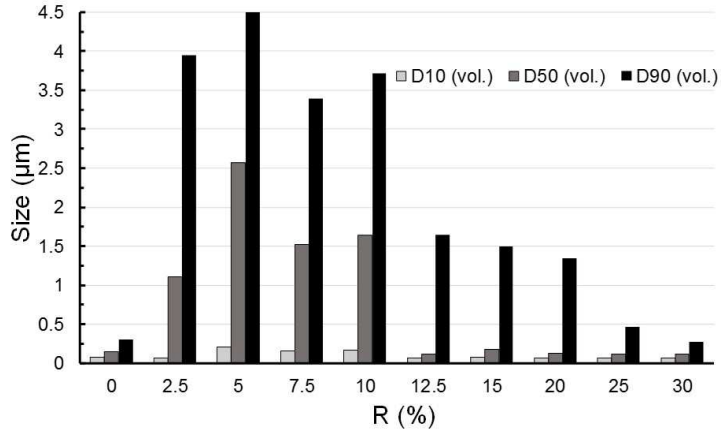

Figure 6: D_{10}, D_{50} and D_{90} (in volume) obtained from particle size measurements for alumina-silica mixtures (pH = 6.5) with various R ratios.

The rheological behavior was evaluated by shear flow measurements only on the most stable suspensions, i.e. for R = 20, 25 and 30%, at pH 6.5, because the instability observed on suspensions at lower R do not allow performing correct and valuable measurements. It is noticeable that rheological measurements were not successful at R = 15%, whereas previous observations show that suspensions are disaggregated for R higher than 12.5%. This observation will be discussed in the last section of Discussion. The results obtained for R = 30% are reported for different solid fractions (from 10 vol.% to 35 vol.%) in Figure 7a). Very similar curves were obtained for binary mixtures with R = 20 and 25% (presented in Supplementary material), with a shear-thinning behavior, leading to a very low and constant viscosity for high shear rates (above 10 s^{-1}). The viscosity increases when the solid fraction increases, but the values remain low, below 0.1 Pa.s, even at a high solid fraction of 35 vol.%. The volume fraction dependence of the high shear viscosity (100 s^{-1}) could be fitted by the Krieger-Dougherty model (Figure 7b)) [46] [47], with η the viscosity of the suspension, η_0 the

viscosity of the solvent, Φ the solid volume fraction of the suspension, Φ_{max} the maximum solid volume fraction, and [η] a fitting parameter (Equation 2):

$$\eta = \eta_0 \left(1 - \frac{\phi}{\phi_{max}}\right)^{-[\eta]\phi_{max}} \qquad \text{Equation 2}$$

With η_0 = 0,001 Pa.s and [η] = 5.4, Φ_{max} = 0.44 was calculated. The result obtained here corresponds to a relatively high maximum solid fraction for a ceramic suspension containing particles whose diameters are much below 1 µm; thus for high ratios, colloidal silica acts as a very efficient inorganic dispersant.

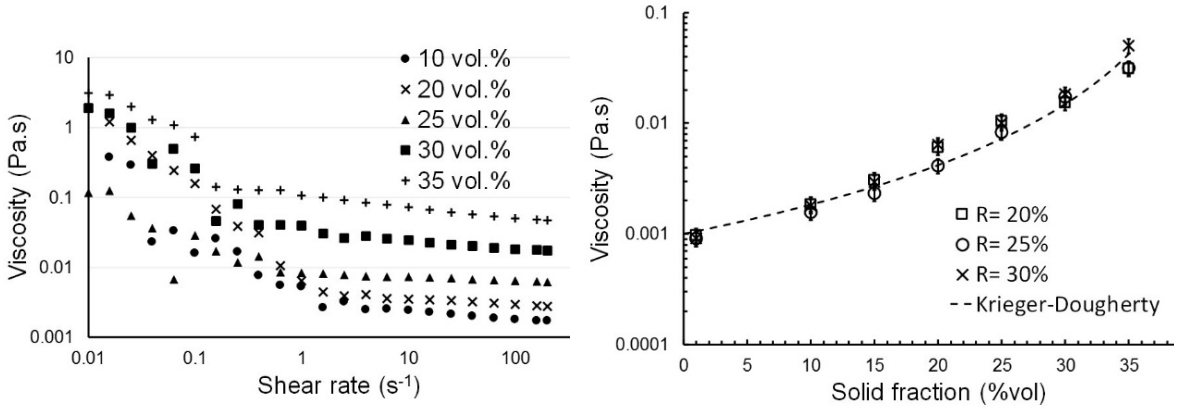

a) b)

Figure 7: a) Shear flow measurements on an alumina-silica suspension (R = 30 %, pH = 6.5) for different solid fractions (from 10 vol.% to 35 vol. %). b) Viscosity measured at 100 s^{-1} on alumina-silica suspensions for R = 20, 25, and 30%, at pH 6.5, as a function of the solid fraction, and a Krieger-Dougherty model.

TEM images of heteroaggregates are presented in Figure 8 for R = 15, 25 and 30%. Images clearly show that silica colloids cover the surface of alumina particles in all cases.

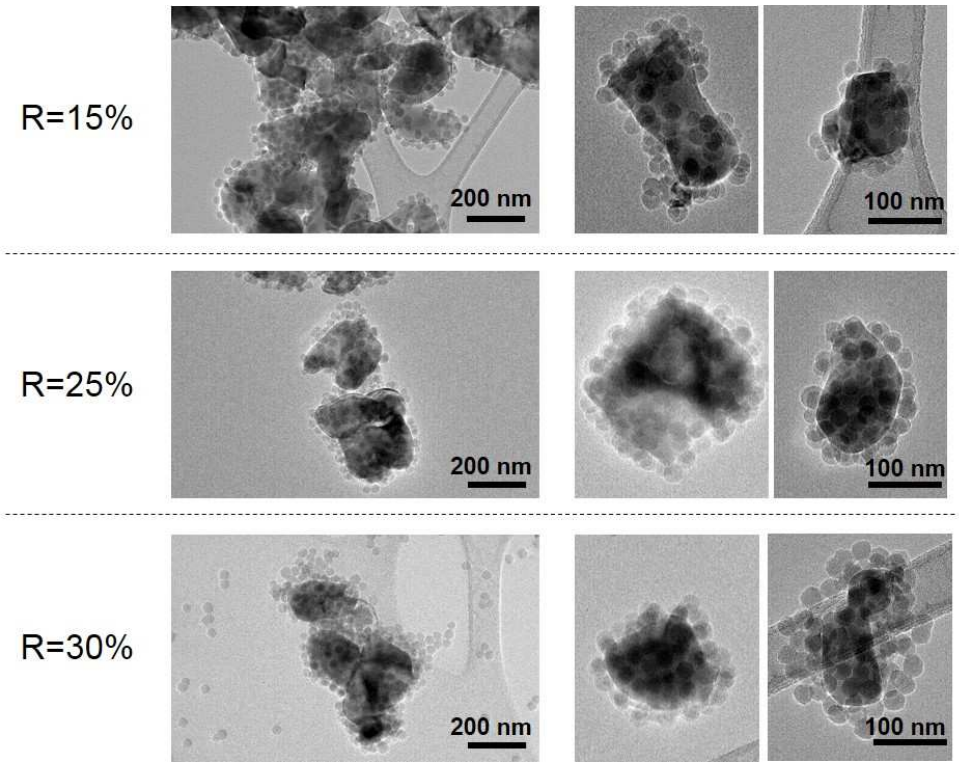

Figure 8: Transmission Electron Microscopy (TEM) images of alumina/silica heteroaggregates, for different R ratios.

In the following, Brownian dynamics simulations will help discussing the heteroaggregation mechanisms in the whole range of R (from 1 to 30%), and as a function of the solid fraction, to better understand particles arrangement and microstructures.

3. Brownian dynamics simulations

3.1. Methodology

The methodology followed to perform the Brownian dynamics simulations is explained in this part. Spherical alumina particles of 206 nm (radius a_1 = 103 nm) and silica nanoparticles of 24 nm (radius a_2 = 12 nm) are considered. In all cases, n_1 = 10 alumina particles are considered. n_2 silica nanoparticles are then inserted according to the different values of R = 1, 6, 8, 10, 15 and 30% which are studied. The number of silica particles used in the simulations is reported in Table 1.

R (%)	1	6	8	10	15	30
n_2	116	730	990	1271	2019	4903

Table 1: Number of silica nanoparticles used in the simulations (n_2) as a function of R (with n_1 = 10 alumina particles).

All simulations are performed considering periodic boundary conditions in a cubic simulation box, whose size (L) is fixed by the particle numbers and the solid volume fraction (Φ) as (Equation 3):

$$L^3 = \frac{4\pi(n_1 a_1^3 + n_2 a_2^3)}{3\phi} \qquad \text{Equation 3}$$

Thus changing the volume fraction of solid is the same as changing the size of the simulation box. At the beginning of the simulations, particles are randomly distributed in the simulation box avoiding superposition. Then the trajectory of each particle is calculated by the Brownian dynamics simulation scheme presented in references [36] and [37]. The motion of the alumina particles is obtained by a full Langevin scheme, whereas the motion of the small silica particles is obtained by integrating the overdamped Langevin equation, in which inertia is neglected. However, when an alumina particle is covered by silica, the heteroaggregate is moved with a two steps procedure. First, it moves as a whole with the diffusion coefficient of an isolated alumina particle considering that the small silica particles are bounded on its surface. Then, in a second step, only the small silica particles move, allowing their rearrangement on the alumina surface. This algorithm is chosen to avoid the caging effect already observed in Brownian dynamics simulations with particles that have a high size ratio and which prevents the diffusion of larger particles surrounded by smaller ones [33] [48]. More details on this simulation scheme can be found in reference [37]. These Brownian dynamics simulations are performed with a time step of $\delta t = 5.10^{-10}$ s.

Interactions between the particles are described by an extension of the D.L.V.O. theory [5]. Interaction is thus the sum of two contributions: an attraction due to van der Waals forces U_{ij}^{vdW} and an electrostatic interaction U_{ij}^{el}

$$U_{ij}^{DLVO} = U_{ij}^{vdW} + U_{ij}^{el} \qquad \text{Equation 4}$$

With [49]:

$$U_{ij}^{vdW} = -\frac{A_{ij}}{6}\left\{\frac{2a_i a_j}{r_{ij}^2-(a_i+a_j)^2} + \frac{2a_i a_j}{r_{ij}^2-(a_i-a_j)^2} + \ln\left[\frac{r_{ij}^2-(a_i+a_j)^2}{r_{ij}^2-(a_i-a_j)^2}\right]\right\} \qquad \text{Equation 5}$$

with a_i the radius of particle i; r_{ij} the center-to-center distance between colloids i and j; and A_{ij} the Hamaker constant : values of 1.48×10^{-20} J, 4.6×10^{-21} J, 4.76×10^{-20} J are considered for the alumina-silica, silica-silica and alumina-alumina interactions respectively [50]. The electrostatic interaction is expressed by the Hogg-Healy-Fuerstenau potential [51]:

$$U_{ij}^{el} = \pi\varepsilon \frac{a_i a_j}{a_i + a_j} \left(\psi_i^2 + \psi_j^2\right) \left\{ \frac{2\psi_i \psi_j}{\psi_i^2 + \psi_j^2} \ln\left[\frac{1+e^{-\kappa h_{ij}}}{1-e^{-\kappa h_{ij}}}\right] + \ln\left[1 - e^{-2\kappa h_{ij}}\right] \right\} \quad \text{Equation 6}$$

where $h_{ij} = r_{ij} - (a_i + a_j)$, $\varepsilon = 81\varepsilon_0$ is the dielectric constant of water, ε_0 is the permittivity of vacuum, Ψ_i is the surface potential of particle i and κ is the inverse of the Debye screening length (no added salt is used in these experiments, therefore the ionic concentration is small and a value of $\kappa = 10^8$ m^{-1} is considered). Experimentally, all the suspensions are prepared at pH 6.5. In order to reproduce their behavior numerically, the surface potential of particles is assimilated to the zeta potential measured experimentally at pH 6.5, therefore $\Psi_1 = 38$ mV and $\Psi_2 = -32$ mV for alumina and silica respectively (see Figure 3). The D.L.V.O. potentials used in the simulations are plotted in Figure 9. The interactions between particles of same nature are repulsive, whereas they are attractive between alumina and silica particles. Because the D.L.V.O. potential diverges at the particles contact, the strategy presented in references [33] [48] is applied. The D.L.V.O. is cut at a well depth of $14k_BT$ (k_B being the Boltzmann constant, and T is the room temperature) and a linear repulsive potential is applied to avoid interpenetration. This strategy is chosen because it has already allowed to quantitatively reproduce silica adsorption on alumina in previous studies [33].

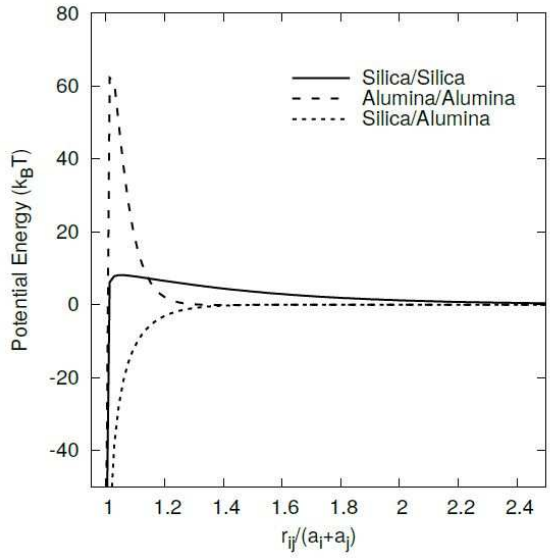

Figure 9: D.L.V.O. potentials used in simulations for silica-silica, alumina-alumina and silica-alumina interactions.

3.2. Numerical results

Snapshots of simulations for various R are shown in Figures 10 and 11. Two different solid fractions are considered, 1 vol.% and 10 vol.%. In all cases, silica nanoparticles are adsorbed on the alumina particles. For the lowest values of R, all the introduced silica nanoparticles are adsorbed on alumina. For the highest values of R, some silica nanoparticles remain in suspension, even though alumina is not completely covered: a saturation of the adsorption of alumina by silica is thus observed. This is in agreement with some results obtained in previous studies [48], and is explained by the repulsive interactions between the adsorbed silica nanoparticles.

In order to quantify the maximum adsorption depending on R, and for the two solid volume fractions (1 vol.% and 10 vol.%), some calculations have been done on 10 independent simulations, as reported in Figure 12. It is observed for both solid fractions, below R = 6%, that all silica nanoparticles are adsorbed at the alumina surface. When R is comprised between [6%-8%], the values for adsorption start deviating from the line of complete adsorption, which means that some nanoparticles cannot adsorb on the alumina surface, and remain in the solvent. Nevertheless the number of silica nanoparticles adsorbed on alumina continues increasing with R. Moreover, the number of nanoparticles adsorbed on alumina also increases with the solid loading. This behavior can be attributed to the repulsive interactions between the adsorbed nanoparticles and the surrounding “free” silica nanoparticles. When the number of surrounding nanoparticles increases, the energy of interactions between the silica nanoparticles increases and adsorbing more silica nanoparticles on alumina may help to decrease the total energy of the system (potential well depth of $-14k_BT$ for the alumina-silica interaction).

Simulation snapshots show that alumina particles can aggregate thanks to the small nanoparticles which bridge them. This is clearly observed for R = 1% at Φ = 1 and 10 vol.% (Figure 10). To characterize this aggregation, the aggregates containing at least one alumina particle are analyzed at t = 0.1s. Figure 13 shows the mean number of alumina particles in the aggregates as a function of R.

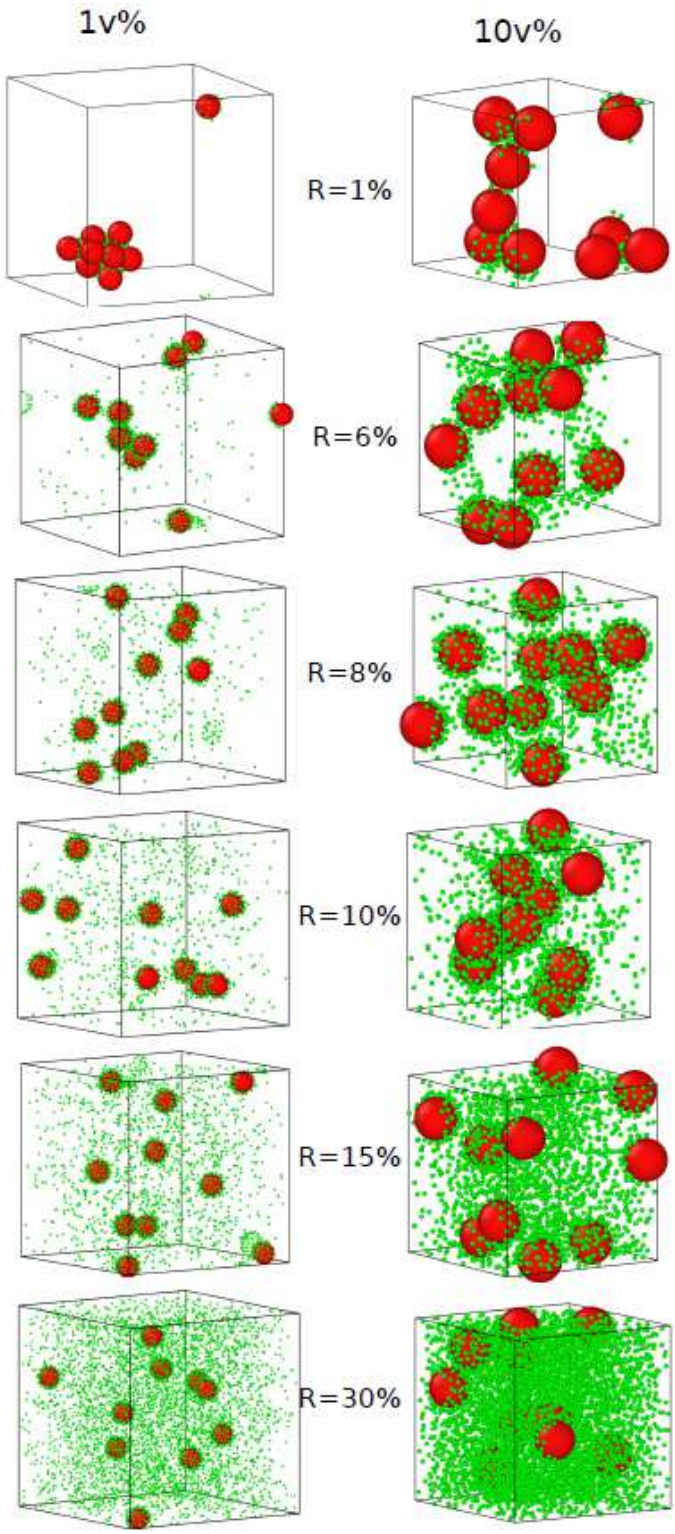

Figure 10: Snapshots of Brownian dynamics simulations at t = 0.1 s for various ratios R of silica nanoparticles: on the left with a solid volume fraction of 1 vol.%, and on the right with a solid volume fraction of 10 vol.%

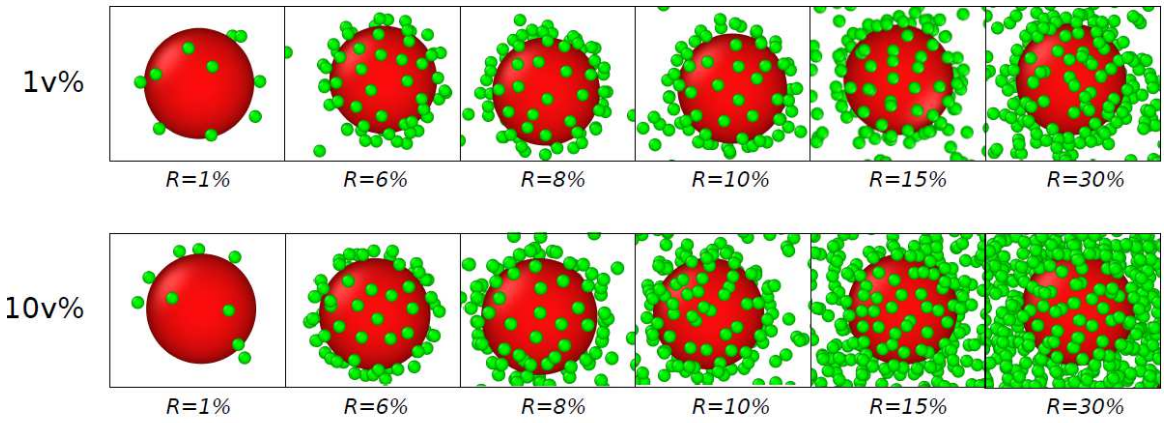

Figure 11: Snapshots of one isolated alumina particle obtained in Brownian dynamics simulations with various ratios R of silica nanoparticles at t = 0.03 s (except for R = 1% at 10 vol.%, t = 0.0015 s)

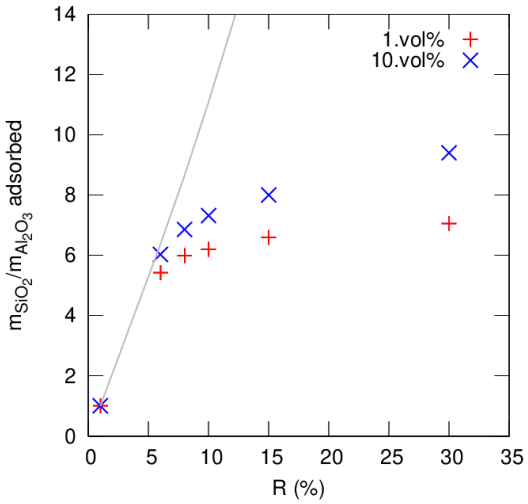

Figure 12: Adsorption isotherm of silica nanoparticles on alumina particles calculated from the simulation results with solid volume fractions of 1 vol.% and 10 vol.%. The grey line indicates complete adsorption. Results are averaged over 10 independent simulations.

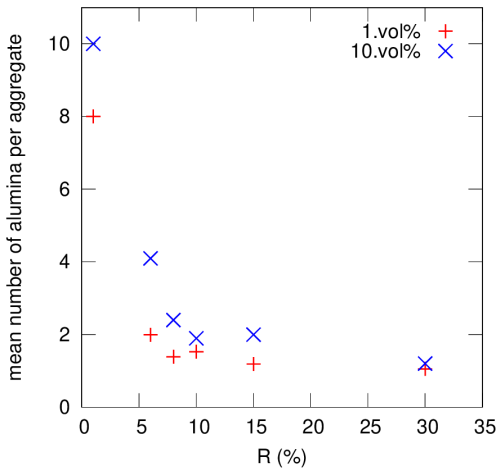

Figure 13: Mean number of alumina particles per aggregate observed at t = 0.1 s as a function of R, for simulations with a solid loading of 1 vol.% (in red) and 10 vol.% (in blue). Results are averaged over 10 independent simulations.

Adding silica nanoparticles (increase of R) allows a better stabilization of the suspensions, traduced by the presence of aggregates containing only one alumina particle, in agreement with experimental characterizations. An increase of R induces not only an increase in the amount of silica adsorbed but also faster adsorption kinetics (see Figure 14). Thus, at the highest R ratios, alumina particles are quickly covered by the silica nanoparticles, which repel each other and thus hinder the aggregation of the alumina particles. Moreover, it can also be noted that a smaller amount of silica is required to stabilize the less concentrated suspensions. For Φ = 10 vol.%, a ratio R = 30% is indeed necessary to mainly have isolated alumina particles, whereas a smaller fraction R = 15% is enough for Φ = 1 vol.%. This can also be explained by the competition between the kinetics of alumina aggregation and the kinetics of silica adsorption. For Φ = 10 vol.%, alumina particles are closer to each other from the beginning of the simulation, and can more easily encounter before their surface is sufficiently covered by silica to avoid their aggregation. This result therefore shows that not only R is important for understanding alumina aggregation but also the solid volume fraction of the suspensions.

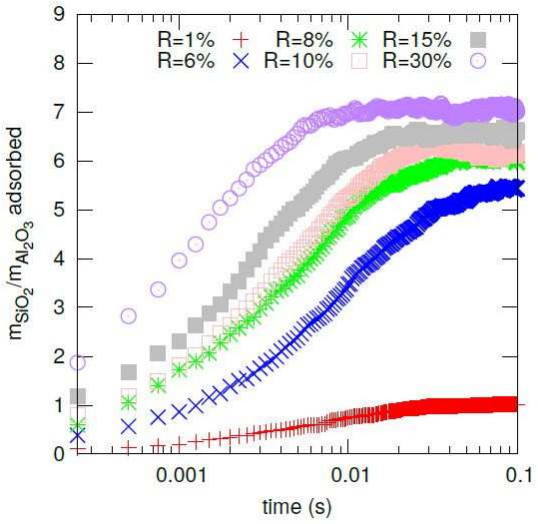

Figure 14: Kinetics of silica nanoparticles adsorption on the surface of alumina particles in simulations with a solid volume fractions of 1 vol.% (curves are not averaged).

4. Discussion

Experimental characterizations and numerical simulations were performed on mixtures of alumina and silica colloids at pH 6.5, where the surface charge was maximum and opposite. A very good agreement was obtained between experiments and simulations. Opposite surface charges lead to the adsorption of small silica colloids at the surface of alumina particles. The simulations show a saturation of the silica adsorption on alumina for R ratios between 6 and 8%. These values are in agreement with the experimental measurements of zeta potentials shown in Figure 4. For values R < 7.5%, a strong decrease in zeta potential is indeed observed which can be explained by the adsorption of negatively charged silica nanoparticles on the surface of the alumina. For the highest values of R, it can be observed that the zeta potential decreases much more slowly with R, the silica particles adsorb with difficulty, which can correspond to an adsorption saturation, as observed in simulations. It can be noticed that these R values are much lower than that necessary to have a hexagonal close packing of silica nanoparticles at the surface of alumina particles. Calculations for hexagonal close packing leads to a surface coverage of $\frac{\pi}{2\sqrt{3}} = 91\%$, and a ratio R = 22.5% (considering a density of $\rho(Al_2O_3)$ = 3.98 g.cm^{-3} and of $\rho(SiO_2)$ = 2.2 g.cm^{-3}, for alumina and silica respectively). This low coverage at the saturation can be explained by the repulsions between the silica particles adsorbed on the surface of the alumina [48] [31]. By considering a compact hexagonal stacking of silica on the surface, we can indeed deduce an effective radius for the silica particles, which

allows to take into account these repulsions between the adsorbed nanoparticles [48] (Equation 7) :

$$\frac{surface\ covered\ by\ effective\ silica\ particles}{surface\ developed\ by\ an\ alumina\ particle} = \frac{r_s\,\pi\,a_{2,eff}{}^2}{4\pi\,(a_1+a_2)^2} = \frac{\pi}{2\sqrt{3}} \qquad \text{Equation 7}$$

with r_s the ratio between the number of adsorbed silica nanoparticles and the number of alumina particles for the saturation of silica adsorption. Values of $a_{2,eff}=2.14a_2$ and $a_{2,eff}=1.83a_2$ are found for R=6% and R=8% respectively, which is much higher than the silica radius a_2. Note that $a_{2,eff} = 1.83a_2$ corresponds to $a_{2,eff} = a_2$ + the Debye length, which is estimated here at 10 nm and which characterizes the range of electrostatic interactions. This study proves that it is fundamental to consider the electrostatic interactions between the smallest particles, here silica, to explain their adsorption at the surface of alumina. The consequence is that a low amount of silica is enough to create a repulsive barrier and stabilize alumina suspensions, even at high solid fractions.

The simulations also reveal that the volume fraction of particles plays a role on the value of the saturation of adsorption and on the aggregation of alumina particles, which is not always considered in the studies previously reported in the literature. For the same values of R, higher than those necessary to have the saturation of silica adsorption, it appears that the suspensions are more aggregated for a volume fraction of 10 vol.% than 1 vol.%. The simulations show indeed that there is a competition between the adsorption kinetics of the silica particles and the aggregation kinetics of the alumina particles. To avoid the aggregation of alumina particles, they must be sufficiently covered with silica particles before meeting each other. This may explain some experimental observations. Indeed, the sedimentation tests (Figure 5) and the measurement of the aggregate sizes (Figure 6) show that for R higher than 12.5%, the suspensions are not aggregated. However, rheological measurements could not be carried out with R = 15% on the whole concentration range (up to Φ = 35 vol.%), due to flocculation. This difference in stability can thus be explained by the volume fraction of the suspensions used in the experiments. Indeed, the sedimentation and aggregate size measurements are carried out on dilute suspensions with a maximum of particles volume fraction of 1 vol.%, whereas the rheology measurements are carried out also with higher volume fractions up to 35 vol.%. According to the simulations, it can thus be expected that in rheology there is more aggregation at R = 15% than in dilute suspensions. This study thus shows that in these binary systems where different kinetics have to be taken into account, the behavior of suspension is complex, and the one observed in dilute suspensions may be different from those observed in concentrated suspensions.

5. Conclusion

Experimental characterizations and numerical simulations were performed on mixtures of alumina particles and silica nanoparticles at pH 6.5, where the colloids surface charge was maximum and opposite. The ratio of silica to the total solid fraction was varied from R = 1 to 30% (in weight). Opposite surface charges lead to the adsorption of the small silica colloids at the surface of alumina particles. For the lowest R, heteroaggregation induces heterocoagulation, i.e. a rapid instability of the suspension and a strong agglomeration, whereas for the highest R, on the contrary, heteroaggregation leads to the dispersion and a long-term stability, at the same pH. The experiments conducted by zeta potential measurements, sedimentation tests, granulometry and rheological measurements, show that the transition from coagulation to dispersion is in the range of R [6-15%]. Simulations performed by Brownian dynamics allow getting a better insight into the mechanism of heteroaggregation as a function of R, and the importance of considering the volume fraction of particles. A very good agreement is obtained between experiments and simulations, which are complementary. Actually, simulations show that silica can totally adsorb at the surface of alumina particles until R = 6%-8%. Then repulsive interactions between silica particles limit their adsorption, less silica is adsorbed, and most of them remain in the solvent, hindering alumina agglomeration by repulsive interactions. The adsorption of silica is governed by electrostatic interactions; if this result was already shown by other authors [48] [31], it has to be noticed that a much larger range of R has been explored in this study. Finally, the second important aspect of this study is to highlight the importance of the particle concentration, which is often not considered in the literature: alumina agglomeration may occur for higher solid fractions, because not enough silica is adsorbed before two alumina particles encounter. This observation is important to properly interpret the different experimental characterizations that are not always performed at the same volume fractions of particles according to the specificities of the experiments. Finally, this paper shows that alumina can be efficiently stabilized by using silica particles, which opens new perspectives for ceramic liquid processing, by using a silica sol at a medium pH and at a moderate concentration to modulate alumina suspension properties without any other organic additives.

Acknowledgment

The authors thank CALI and its team for providing the computational facilities (CALI has been financed by the region Limousin, the institutes XLIM, IPAM, GEIST, and the University of Limoges). Figures 10 and 11 have been obtained thanks to the software OVITO [52].

References

[1] B. Derjaguin and L. Landau, "Theory of the stability of strongly charged lyophobic sols and of the adhesion of strongly charged particles in solutions of electrolytes," *Prog. Surf. Sci.*, vol. 43, no. 1–4, pp. 30–59, 1993, doi: 10.1016/0079-6816(93)90013-L.

[2] J. A. Maroto and F. J. de las Nieves, "Optimization of the heterocoagulation process of polymer colloids with different particle size," *Colloids Surf. Physicochem. Eng. Asp.*, vol. 96, no. 1, pp. 121–133, Mar. 1995, doi: 10.1016/0927-7757(94)03048-5.

[3] A. M. Islam, B. Z. Chowdhry, and M. J. Snowden, "Heteroaggregation in colloidal dispersions," *Adv. Colloid Interface Sci.*, vol. 62, no. 2, pp. 109–136, Dec. 1995, doi: 10.1016/0001-8686(95)00276-V.

[4] J. M. López-López, A. Schmitt, A. Moncho-Jordá, and R. Hidalgo-Álvarez, "Stability of binary colloids: kinetic and structural aspects of heteroaggregation processes," *Soft Matter*, vol. 2, no. 12, pp. 1025–1042, Nov. 2006, doi: 10.1039/B608349H.

[5] M. Elimelech, X. Jia, J. Gregory, and R. Williams, *Particle Deposition and Aggregation: Measurement, Modelling and Simulation*. Elsevier, 1998.

[6] D. Zhou, A. I. Abdel-Fattah, and A. A. Keller, "Clay Particles Destabilize Engineered Nanoparticles in Aqueous Environments," *Environ. Sci. Technol.*, vol. 46, no. 14, pp. 7520–7526, Jul. 2012, doi: 10.1021/es3004427.

[7] J. T. K. Quik, I. Velzeboer, M. Wouterse, A. A. Koelmans, and D. van de Meent, "Heteroaggregation and sedimentation rates for nanomaterials in natural waters," *Water Res.*, vol. 48, pp. 269–279, Jan. 2014, doi: 10.1016/j.watres.2013.09.036.

[8] E. Besseling, J. T. K. Quik, M. Sun, and A. A. Koelmans, "Fate of nano- and microplastic in freshwater systems: A modeling study," *Environ. Pollut.*, vol. 220, pp. 540–548, Jan. 2017, doi: 10.1016/j.envpol.2016.10.001.

[9] E. Duguet, A. Désert, A. Perro, and S. Ravaine, "Design and elaboration of colloidal molecules: an overview," *Chem. Soc. Rev.*, vol. 40, no. 2, pp. 941–960, Jan. 2011, doi: 10.1039/C0CS00048E.

[10] M. Zanini, C.-P. Hsu, T. Magrini, E. Marini, and L. Isa, "Fabrication of rough colloids by heteroaggregation," *Colloids Surf. Physicochem. Eng. Asp.*, vol. 532, pp. 116–124, Nov. 2017, doi: 10.1016/j.colsurfa.2017.05.084.

[11] T. Garino, "Heterocoagulation as an Inclusion Coating Technique for Ceramic Composite Processing," *J. Am. Ceram. Soc.*, vol. 75, no. 3, pp. 514–518, 1992, doi: 10.1111/j.1151-2916.1992.tb07835.x.

[12] G. L. Drisko and C. Sanchez, "Hybridization in Materials Science – Evolution, Current State, and Future Aspirations," *Eur. J. Inorg. Chem.*, vol. 2012, no. 32, pp. 5097–5105, Nov. 2012, doi: 10.1002/ejic.201201216.

[13] V. Uricanu, J. R. Eastman, and B. Vincent, "Stability in Colloidal Mixtures Containing Particles with a Large Disparity in Size," *J. Colloid Interface Sci.*, vol. 233, no. 1, pp. 1–11, Jan. 2001, doi: 10.1006/jcis.2000.7192.

[14] D. Morphew and D. Chakrabarti, "Clusters of anisotropic colloidal particles: From colloidal molecules to supracolloidal structures," *Curr. Opin. Colloid Interface Sci.*, vol. 30, pp. 70–80, Jul. 2017, doi: 10.1016/j.cocis.2017.05.006.

[15] M. Maas, C. C. Silvério, J. Laube, and K. Rezwan, "Electrostatic assembly of zwitterionic and amphiphilic supraparticles," *J. Colloid Interface Sci.*, vol. 501, pp. 256–266, Sep. 2017, doi: 10.1016/j.jcis.2017.04.076.

[16] W. Li, H. Palis, R. Mérindol, J. Majimel, S. Ravaine, and E. Duguet, "Colloidal molecules and patchy particles: complementary concepts, synthesis and self-assembly," *Chem. Soc. Rev.*, vol. 49, no. 6, pp. 1955–1976, Mar. 2020, doi: 10.1039/C9CS00804G.

[17] V. M. Shalaev, "Optical negative-index metamaterials," *Nat. Photonics*, vol. 1, no. 1, pp. 41–48, Jan. 2007, doi: 10.1038/nphoton.2006.49.

[18] F. Li, D. P. Josephson, and A. Stein, “Colloidal Assembly: The Road from Particles to Colloidal Molecules and Crystals,” *Angew. Chem. Int. Ed.*, vol. 50, no. 2, pp. 360–388, 2011, doi: 10.1002/anie.201001451.
[19] A. F. Demirörs, M. T. Akan, E. Poloni, and A. R. Studart, “Active cargo transport with Janus colloidal shuttles using electric and magnetic fields,” *Soft Matter*, vol. 14, no. 23, pp. 4741–4749, Jun. 2018, doi: 10.1039/C8SM00513C.
[20] B. P. Binks, W. Liu, and J. A. Rodrigues, “Novel Stabilization of Emulsions via the Heteroaggregation of Nanoparticles,” *Langmuir*, vol. 24, no. 9, pp. 4443–4446, May 2008, doi: 10.1021/la800084d.
[21] M. Cerbelaud, A. Aimable, and A. Videcoq, “Role of Electrostatic Interactions in Oil-in-Water Emulsions Stabilized by Heteroaggregation: An Experimental and Simulation Study,” *Langmuir*, vol. 34, no. 51, pp. 15795–15803, Dec. 2018, doi: 10.1021/acs.langmuir.8b02922.
[22] S. Upendar, E. Mani, and M. G. Basavaraj, “Aggregation and Stabilization of Colloidal Spheroids by Oppositely Charged Spherical Nanoparticles,” *Langmuir*, vol. 34, no. 22, pp. 6511–6521, Jun. 2018, doi: 10.1021/acs.langmuir.8b00645.
[23] A. Pringuet, C. Pagnoux, A. Videcoq, and J.-F. Baumard, “Granulating fine powders into millimetric spheres with a multiscale porosity: The case of titania,” *Microporous Mesoporous Mater.*, vol. 140, no. 1, pp. 17–24, Apr. 2011, doi: 10.1016/j.micromeso.2010.09.005.
[24] L. Ploux *et al.*, “New colloidal fabrication of bioceramics with controlled porosity for delivery of antibiotics,” *J. Mater. Sci.*, vol. 51, no. 19, pp. 8861–8879, Oct. 2016, doi: 10.1007/s10853-016-0133-z.
[25] M. Cerbelaud, M. Muñoz, F. Rossignol, and A. Videcoq, “Self-Organization of Large Alumina Platelets and Silica Nanoparticles by Heteroaggregation and Sedimentation: Toward an Alternative Shaping of Nacre-Like Ceramic Composites,” *Langmuir*, vol. 36, no. 13, pp. 3315–3322, Apr. 2020, doi: 10.1021/acs.langmuir.0c00170.
[26] H. Kihira, N. Ryde, and E. Matijević, “Kinetics of heterocoagulation. Part.2—The effect of the discreteness of surface charge,” *J. Chem. Soc. Faraday Trans.*, vol. 88, no. 16, pp. 2379–2386, Jan. 1992, doi: 10.1039/FT9928802379.
[27] N. Ryde and E. Matijević, “Kinetics of heterocoagulation. Part 4.—Evaluation of absolute coagulation rate constants using a classical light scattering technique,” *J. Chem. Soc. Faraday Trans.*, vol. 90, no. 1, pp. 167–171, Jan. 1994, doi: 10.1039/FT9949000167.
[28] M. L. Fisher, M. Colic, M. P. Rao, and F. F. Lange, “Effect of Silica Nanoparticle Size on the Stability of Alumina/Silica Suspensions,” *J. Am. Ceram. Soc.*, vol. 84, no. 4, pp. 713–718, 2001, doi: 10.1111/j.1151-2916.2001.tb00731.x.
[29] W. Lin, M. Kobayashi, M. Skarba, C. Mu, P. Galletto, and M. Borkovec, “Heteroaggregation in Binary Mixtures of Oppositely Charged Colloidal Particles,” *Langmuir*, vol. 22, no. 3, pp. 1038–1047, Jan. 2006, doi: 10.1021/la0522808.
[30] S. Rollié and K. Sundmacher, “Determination of Cluster Composition in Heteroaggregation of Binary Particle Systems by Flow Cytometry,” *Langmuir*, vol. 24, no. 23, pp. 13348–13358, Dec. 2008, doi: 10.1021/la8024765.
[31] J. F. Gilchrist, A. T. Chan, E. R. Weeks, and J. A. Lewis, “Phase Behavior and 3D Structure of Strongly Attractive Microsphere−Nanoparticle Mixtures,” *Langmuir*, vol. 21, no. 24, pp. 11040–11047, Nov. 2005, doi: 10.1021/la051998k.
[32] J. Lee, S. J. Lee, K. H. Ahn, and S. J. Lee, “Nanoparticle-Induced Gelation of Bimodal Slurries with Highly Size-Asymmetric Particles: Effect of Surface Chemistry and Concentration,” *Langmuir*, vol. 31, no. 51, pp. 13639–13646, Dec. 2015, doi: 10.1021/acs.langmuir.5b03752.
[33] M. Cerbelaud, A. Videcoq, P. Abélard, and R. Ferrando, “Simulation of the heteroagglomeration between highly size-asymmetric ceramic particles,” *J. Colloid Interface Sci.*, vol. 332, no. 2, pp. 360–365, Apr. 2009, doi: 10.1016/j.jcis.2008.11.063.
[34] M. Cerbelaud, A. Videcoq, P. Abélard, C. Pagnoux, F. Rossignol, and R. Ferrando, “Self-assembly of oppositely charged particles in dilute ceramic suspensions: predictive role of simulations,” *Soft Matter*, vol. 6, no. 2, pp. 370–382, Jan. 2010, doi: 10.1039/B908671D.

[35] M. A. Piechowiak *et al.*, “Oppositely Charged Model Ceramic Colloids: Numerical Predictions and Experimental Observations by Confocal Laser Scanning Microscopy,” *Langmuir*, vol. 26, no. 15, pp. 12540–12547, Aug. 2010, doi: 10.1021/la101027d.
[36] A. Laganapan, M. Cerbelaud, R. Ferrando, C. T. Tran, B. Crespin, and A. Videcoq, “Computer simulations of heteroaggregation with large size asymmetric colloids,” *J. Colloid Interface Sci.*, vol. 514, pp. 694–703, Mar. 2018, doi: 10.1016/j.jcis.2017.12.071.
[37] C. T. Tran, B. Crespin, M. Cerbelaud, and A. Videcoq, *Brownian Dynamics Simulation on the GPU: Virtual Colloidal Suspensions*. The Eurographics Association, 2015.
[38] P. Garcia-Perez, C. Pagnoux, A. Pringuet, A. Videcoq, and J. F. Baumard, “Agglomeration of alumina submicronparticles by silica nanoparticles: Application to processing spheres by colloidal route,” *J. Colloid Interface Sci.*, vol. 313, no. 2, pp. 527–536, Sep. 2007, doi: 10.1016/j.jcis.2007.04.050.
[39] P. Garcia-Perez, C. Pagnoux, F. Rossignol, and J.-F. Baumard, “Heterocoagulation between SiO2 nanoparticles and Al2O3 submicronparticles; influence of the background electrolyte,” *Colloids Surf. Physicochem. Eng. Asp.*, vol. 281, no. 1, pp. 58–66, Jun. 2006, doi: 10.1016/j.colsurfa.2006.02.018.
[40] A. Pringuet, C. Pagnoux, A. Videcoq, and J.-F. Baumard, “Granulating Titania Powder by Colloidal Route Using Polyelectrolytes,” *Langmuir*, vol. 24, pp. 10702–8, Oct. 2008, doi: 10.1021/la8009578.
[41] C. Pagnoux, N. Tessier-Doyen, A. Pringuet, M. Cerbelaud, and P. Garcia-Perez, “Influence of the suspension flocculated state on the microstructure of alumina spheres elaborated by colloidal granulation,” *J. Eur. Ceram. Soc.*, vol. 29, no. 8, pp. 1379–1385, May 2009, doi: 10.1016/j.jeurceramsoc.2008.09.007.
[42] S. Ananthakumar, V. Raja, and K. G. K. Warrier, “Effect of nanoparticulate boehmite sol as a dispersant for slurry compaction of alumina ceramics,” *Mater. Lett.*, vol. 43, no. 4, pp. 174–179, Apr. 2000, doi: 10.1016/S0167-577X(99)00255-4.
[43] X. Zhu, D. Jiang, S. Tan, and Z. Zhang, “Dispersion properties of alumina powders in silica sol,” *J. Eur. Ceram. Soc.*, vol. 21, no. 16, pp. 2879–2885, Dec. 2001, doi: 10.1016/S0955-2219(01)00229-1.
[44] D. Kong, H. Yang, Y. Yang, S. Wei, J. Wang, and B. Cheng, “Dispersion behavior and stabilization mechanism of alumina powders in silica sol,” *Mater. Lett.*, vol. 58, no. 27, pp. 3503–3508, Nov. 2004, doi: 10.1016/j.matlet.2004.06.060.
[45] T. E. Petroff, M. Sayer, and S. A. M. Hesp, “Zeta potential modification of ceramic powders using zirconium hydrogel,” *Colloids Surf. Physicochem. Eng. Asp.*, vol. 78, pp. 235–243, Oct. 1993, doi: 10.1016/0927-7757(93)80329-D.
[46] I. M. Krieger and T. J. Dougherty, “A Mechanism for Non-Newtonian Flow in Suspensions of Rigid Spheres,” *Trans. Soc. Rheol.*, vol. 3, no. 1, pp. 137–152, Mar. 1959, doi: 10.1122/1.548848.
[47] L. Bergström, “Shear thinning and shear thickening of concentrated ceramic suspensions,” *Colloids Surf. Physicochem. Eng. Asp.*, vol. 133, no. 1, pp. 151–155, Feb. 1998, doi: 10.1016/S0927-7757(97)00133-7.
[48] M. Cerbelaud, A. Videcoq, P. Abélard, C. Pagnoux, F. Rossignol, and R. Ferrando, “Heteroaggregation between Al2O3 Submicrometer Particles and SiO2 Nanoparticles: Experiment and Simulation,” *Langmuir*, vol. 24, no. 7, pp. 3001–3008, Apr. 2008, doi: 10.1021/la702104u.
[49] J. Lyklema, *Fundamentals of Interface and Colloid Science - 1st Edition*. Academic Press, 1991.
[50] L. Bergström, “Hamaker constants of inorganic materials,” *Adv. Colloid Interface Sci.*, vol. 70, pp. 125–169, Jul. 1997, doi: 10.1016/S0001-8686(97)00003-1.
[51] R. Hogg, T. W. Healy, and D. W. Fuerstenau, “Mutual coagulation of colloidal dispersions,” *Trans. Faraday Soc.*, vol. 62, no. 0, pp. 1638–1651, Jan. 1966, doi: 10.1039/TF9666201638.
[52] A. Stukowski, “Visualization and analysis of atomistic simulation data with OVITO–the Open Visualization Tool,” *Model. Simul. Mater. Sci. Eng.*, vol. 18, no. 1, p. 015012, Dec. 2009, doi: 10.1088/0965-0393/18/1/015012.